AIAA JOURNAL
Vol. 38, No. 2, February 2000

Numerical Study of Shock-Reflection Hysteresis in an Underexpanded Jet

B. J. Gribben,* K. J. Badcock,† and B. E. Richards‡
University of Glasgow, Glasgow, Scotland G12 8QQ, United Kingdom

Shock-reflection hysteresis and plume structure in a low-density, axisymmetric highly underexpanded air jet is examined using a Navier–Stokes flow solver. This type of jet is found in a number of applications, e.g., rocket exhausts and fuel injectors. The plume structure is complex, involving the interaction of several flow features, making this a demanding problem. Two types of shock reflection appear to occur in the plume, regular and Mach, depending on the jet pressure ratio. The existence of a dual solution domain where either type may occur has been predicted, in agreement with experiment where the same phenomenon has been observed for a nitrogen jet. There is a hysteresis in the shock-reflection type; the reflection type observed in the dual-solution domain depends on the time history of the plume development. A quasi-steady approach is employed to calculate the entire hysteresis loop. An implicit, multiblock structured, finite volume flow solver is used. The results of the computational study are used to examine the structure of the plume and are compared with experimental data where possible. Some flow features not initially recognized from experiment have been identified, notably curvature of the Mach disk, recirculation behind the Mach disk, and the regular reflection having Mach-reflection characteristics.

Nomenclature

a	= sound speed
D	= nozzle throat diameter
E	= specific total energy
$\boldsymbol{F}^i$, $\boldsymbol{G}^i$	= convective fluxes
$\boldsymbol{F}^v$, $\boldsymbol{G}^v$	= viscous-diffusive fluxes
H	= specific total enthalpy
$\boldsymbol{H}$	= axisymmetric source vector
M	= Mach number
p	= static pressure
q_i	= heat flux vector
R	= radial distance from plume axis
Re	= throat Reynolds number
r, z, θ	= cylindrical coordinates
s	= entropy
t	= time
v_r, v_z, v_θ	= cylindrical velocity components
$\boldsymbol{W}$	= vector of conservative variables
X	= axial distance from nozzle exit
X_{sr}	= shock reflection distance
γ	= ratio of specific heats
ρ	= density
τ_{ij}	= shear stress tensor

Subscripts

b	= background stagnation conditions
i	= nozzle inlet conditions
r	= reservoir stagnation conditions

I. Introduction

A JET is underexpanded if the gas pressure at the nozzle exit is greater than the ambient pressure. The plumes of highly underexpanded jets are characterized by a complex repeated shock structure. Several examples of real flows where knowledge of the behavior of this type of jet is necessary can be found in the literature, for example, rocket exhausts, fuel injectors, vehicle maneuvering thrusters, and aeroacoustic and aerothermodynamic experiments (see Ref. 1 for a summary). The experimental studies of Crist et al.[2] and Abbett[3] established the basic wave structure of a highly underexpanded jet plume and that regular or Mach reflection may occur depending on the conditions (see Fig. 1 for schematic drawings of regular and Mach reflection flow structure for planar flow). The method of characteristics has been employed by many authors[3–6] in an attempt to develop predictive models for the core expansion and Mach disk location.

A phenomenon associated with low-density highly underexpanded jets that has yet to be fully understood is shock-reflection hysteresis as reported by Welsh.[7] For a (laminar) nitrogen jet exhausting from a nominally Mach 3 nozzle, a set of conditions exist at which either regular reflection (RR) or Mach reflection (MR) may occur depending on the history of the plume development. The regular reflection should be properly termed an apparent regular reflection, for reasons to be discussed in Sec. IV.C, but until then RR will be used for simplicity. Because the reflection type strongly influences the interaction of the jet with its environment, an understanding of the phenomenon and definition of the hysteresis loop limits are important. Quantitative experimental investigation of this problem, aside from being expensive, suffers from probe interference with the jet structure, necessitating the development of nonintrusive measurement techniques.[7] However, these promising methods have yet to reach full maturity, and the potential of a computational fluid dynamics (CFD) analysis is clear, providing the motivation for this study.

The existence of a hysteresis effect in the type of reflection of a two-dimensional oblique shock wave at a wall or symmetric line has been established in recent years. The reflection of the oblique shock wave may take the form of a RR or MR. The type of reflection that occurs depends on the Mach number upstream of the incident shock and the shock angle. However, there is a dual-solution domain where either type may occur and the solution exhibits a hysteresis effect. More background on shock-reflection hysteresis can be found in the review paper[8] and in the description of an experimental[9] and a numerical[10] study.

Axisymmetric Euler and Navier–Stokes solvers have been used to obtain solutions for underexpanded jet plumes with impressive results.[11–14] These calculations demonstrate good agreement with experiment for a wide range of conditions using parameters such as Mach disk location and centerline velocity and are reported to capture the complex wave structure in detail. The authors are unaware of any previous CFD study of the hysteresis phenomenon in underexpanded jets. The hysteresis phenomenon associated with two-dimensional shock reflection has been successfully modeled

Received 31 August 1998; revision received 20 April 1999; accepted for publication 13 July 1999.

*Research Student, Department of Aerospace Engineering.
†Lecturer, Department of Aerospace Engineering.
‡Professor, Department of Aerospace Engineering. Associate Fellow AIAA.

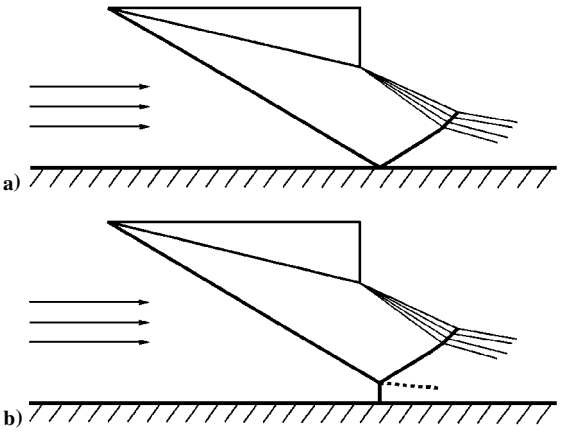

Fig. 1 Schematic diagrams of a) regular reflection and b) Mach reflection using a wedge shock generator.

by using different numerical[15,16] schemes. In this case the crucial quantities (upstream Mach number and incident shock angle) are relatively easy to control and model correctly in a computational approach. However, in the case of shock reflection in the underexpanded jet, these quantities are inherent parts of the calculation rather than being known a priori. All of the interacting features of the complex flowfield must be resolved accurately, making this problem far more demanding. This paper describes how a Navier–Stokes solver has been used in an attempt to model and examine this phenomenon.

II. Numerical Method

The laminar axisymmetric Navier–Stokes equations are written in cylindrical coordinates (r, z, θ) as

$$\frac{\partial \boldsymbol{W}}{\partial t} + \frac{\partial(\boldsymbol{F}^i - \boldsymbol{F}^v)}{\partial r} + \frac{\partial(\boldsymbol{G}^i - \boldsymbol{G}^v)}{\partial z} = \frac{\boldsymbol{H} - \boldsymbol{F}^i + \boldsymbol{F}^v}{r} \qquad (1)$$

where $\boldsymbol{W}$ denotes the vector of conservative variables

$$\boldsymbol{W} = \begin{pmatrix} \rho \\ \rho v_r \\ \rho v_z \\ \rho E \end{pmatrix}$$

$\boldsymbol{F}^i$ and $\boldsymbol{G}^i$ the convective fluxes

$$\boldsymbol{F}^i = \begin{pmatrix} \rho v_r \\ \rho v_r^2 + p \\ \rho v_r v_z \\ \rho v_r H \end{pmatrix}, \qquad \boldsymbol{G}^i = \begin{pmatrix} \rho v_z \\ \rho v_r v_z \\ \rho v_z^2 + p \\ \rho v_z H \end{pmatrix}$$

$\boldsymbol{F}^v$ and $\boldsymbol{G}^v$ the viscous-diffusive fluxes

$$\boldsymbol{F}^v = \begin{pmatrix} 0 \\ \tau_{rr} \\ \tau_{rz} \\ v_r \tau_{rr} + v_z \tau_{rz} + q_r \end{pmatrix}, \qquad \boldsymbol{G}^v = \begin{pmatrix} 0 \\ \tau_{rz} \\ \tau_{zz} \\ v_r \tau_{rz} + v_z \tau_{zz} + q_z \end{pmatrix}$$

and $\boldsymbol{H}$ the axisymmetric source vector

$$\boldsymbol{H} = \begin{pmatrix} 0 \\ p - \tau_{\theta\theta} \\ 0 \\ 0 \end{pmatrix}$$

The shear-stress tensor and heat-flux vector componenets τ_{ij} and q_i are defined in the usual manner. The main features of the Navier–Stokes solver used are outlined here; a detailed description is available elsewhere.[17–19] A cell-centered finite volume method is employed. Osher's scheme and MUSCL variable interpolation are used to discretize the convective terms and central differencing for the diffusive terms. The linear system arising at each implicit time step is solved using a generalized conjugate gradient method. A block incomplete lower-upper (BILU) factorization is used as a preconditioner. A structured multiblock grid system is employed. An important feature of the flow solver is the use of approximate Jacobian matrices for the left-hand side of the linear system. This has led to substantial reductions in memory and CPU-time requirements compared to the use of exact Jacobians.

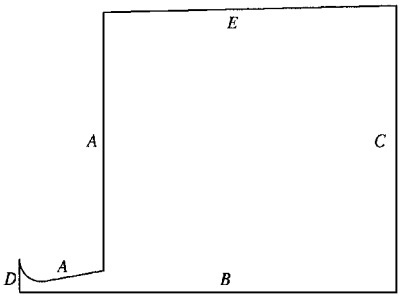

Fig. 2 Boundary conditions.

For this study the assumption is made throughout that the working gas is in the continuum regime with no condensation and has constant specific heats. These assumptions are confirmed by the Aerophysics Group at the Defense Evaluation and Research Agency (DERA) Farnborough, Farnborough, England, United Kingdom, where the experiments were carried out.

Figure 2 shows a diagram of the computational domain with labelled boundary condition types (the size of the nozzle is exaggerated for clarity). The boundaries labeled A denote adiabatic wall boundaries with no slip and zero normal pressure gradient. At B a symmetry condition was applied. To decide which boundary conditions to apply at C, we have the advantage that across all of this boundary we know that we should have outflow. In keeping with an inviscid characteristic analysis, the flow variables are extrapolated from the interior of the domain except for the case of locally subsonic outflow, where the pressure was imposed at the background level. The boundary condition treatment at the nozzle inlet D requires a somewhat more involved treatment. We know the reservoir stagnation conditions (denoted here by r) but require boundary conditions for the nozzle inlet i. This is achieved by assuming that the total enthalpy and entropy are the same for the reservoir and nozzle inlet, thus obtaining expressions for p_i and ρ_i, which are imposed. The velocity components are extrapolated from the interior of the domain. Note that assuming constant entropy s implies a constant entropy measure S defined by

$$S = p/\rho^\gamma$$

For convenience the nondimensionalization is constructed such that

$$\rho_r = 1, \qquad p_r = 1/\gamma \qquad (2)$$

are the values of density and pressure, respectively, in the reservoir. The reservoir sound speed, total enthalpy, and the entropy measure are then

$$a_r = 1, \qquad H_r = 1/(\gamma - 1), \qquad S_r = 1/\gamma$$

We now have two conditions to impose at the inlet i:

$$H_r = \frac{\gamma p_i}{(\gamma - 1)\rho_i} + \frac{(v_r)_i^2 + (v_z)_i^2}{2}, \qquad S_r = \frac{p_i}{\rho_i^\gamma}$$

The velocity components $(v_r)_i$ and $(v_z)_i$ are extrapolated from the interior of the domain. The inlet density and pressure are then

$$\rho_i = \left[1 - \frac{(v_r)_i^2 + (v_z)_i^2}{2}(\gamma - 1)\right], \qquad p_i = \frac{1}{\gamma}\rho_i^\gamma$$

For the boundary condition treatment at E, the background stagnation conditions are known, but the flow direction is not known a priori. With this being similar to the nozzle inlet boundary, the boundary conditions here are treated in the same manner except that

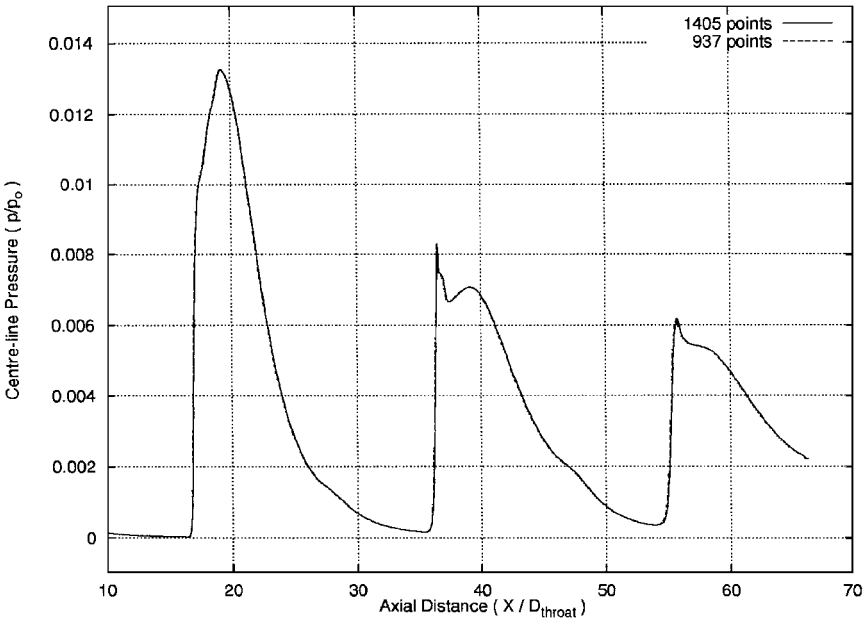

Fig. 3 Result of grid-convergence study (varying the number of points in the axial direction) for $p_0/p_b = 285.7$.

background conditions are used instead of the reservoir conditions in Eqs. (2).

The grid generation for this case is straightforward because of the simple geometry. The computational domain extends 70 nozzle throat diameters downstream in order to capture at least two shock cells and 20 diameters radially from the symmetric line. The grid within the nozzle consists of 58 and 21 points in the axial and radial directions, respectively, with this number having been determined from a grid-convergence study carried out independently of the plume calculations. The plume calculations were also performed using a number of grids. The grid was successively refined until the location of the limits of the dual-solution domain (see the following) became converged, with respect to the number of grid points, to four significant figures. This criterion was selected for the grid-convergence study because it is dependent on the resolution of the plume structure. A grid-converged solution was obtained using 937 and 65 points in the axial and radial directions, respectively.[1] For any given pressure ratio the grid is excessively fine in places, but because the location of the shock reflections vary widely with pressure ratio and the same grid was used in each case this was unavoidable without using grid adaption. The centerline pressure distribution on this grid for one pressure ratio is compared with that obtained on a finer grid in Fig. 3. The excellent agreement supports the claim that the grid used in this study produces numerically accurate results.

III. Shock-Reflection Hysteresis

Welsh[7] describes a series of experiments where the effect of varying the ratio of reservoir stagnation pressure p_r to ambient background pressure p_b on the plume of a highly underexpanded nitrogen jet is examined. The reported shock-reflection hysteresis phenomenon provided the motivation for this CFD study. In the experiments, p_r was varied and p_b was kept constant. In this way the nozzle exit conditions (nominally Mach 3) as well as the pressure ratio were varied. In addition, experiments were carried out for a number of values of p_b and for two different nozzle sizes with throat diameters D of 5 and 15 mm. It is difficult then to isolate the effect of the varying pressure ratio; the location of the dual-solution domain, in terms of pressure ratio and length of the first shock cell, varies widely for the different experimental setups. A number of nozzle calculations covering the experimental range of conditions, as a preliminary to this main study, confirmed that a varying reservoir stagnation pressure has a very large effect on the nozzle exit conditions.[1] With this in mind, the present calculations were performed with a constant nozzle throat Reynolds number Re of 4000 (implying a constant reservoir stagnation pressure) and a varying background pressure. In this way the nozzle exit conditions are constant, enabling examination of the pressure ratio influence independently. Comparison will be made here with the experimental conditions where the value of Re in the reported dual-solution domain is closest to our constant value, namely, the case with $D = 15$ mm, $p_b = 35$ mtorr, where the value of Re varies between approximately 3500 and 4500 in the dual-solution domain.

The nozzle solution provided initial conditions for the full problem. Calculations were performed over a range of pressure ratios from well inside the regular reflection range to well inside the Mach-reflection range including the hysteresis loop. A quasi-steady approach was employed to account for time history effects. First, converged solutions were obtained for a low- and a high-pressure ratio value, these values marking the extremities of the range to be covered. These were used as initial solutions for a calculation with a small change in pressure ratio, thus beginning to traverse the range; this solution being used subsequently as the next initial solution and so on. By using a small step change in pressure ratio between calculations, this approach is very robust and converges quickly at each condition. Obtaining a converged solution (without the aid of a close initial solution) for the end points of the pressure ratio range is far more demanding, requiring approximately 30 times the computational effort. The step change in pressure ratio used is 2.857, corresponding to a step change in reservoir stagnation pressure of 0.1 torr for a background pressure of 35 mtorr in terms of the original experiments.

The calculated shock-reflection type and distance variation with pressure ratio is shown in Fig. 4. The shock-reflection distance is the axial distance (X_{sr}) from the nozzle exit to the center of the first centerline RR or Mach disk, nondimensionalized with respect to the nozzle throat diameter. The figure shows how for a small range of pressure ratios either RR or MR may occur. A description of the plume structures associated with RR and MR is given in Sec. IV. Which condition prevails depends on the time history of the plume development, in accordance with experimental observation. Selecting, for example, the pressure ratio value of 300 in Fig. 4, the corresponding point on the RR(MR) curve will be reached if the condition immediately prior was also on the RR(MR) curve. The arrows on the figure indicate the flip in reflection type, which occurs at the limits of the hysteresis loop. From Fig. 4 the conclusion can be made that the quasi-steady approach has been successful, at least qualitatively, in modeling the shock-reflection hysteresis phenomenon. Included in Fig. 4 is the location of the hysteresis loop for the experimental conditions closest to the constant Reynolds number employed in the calculation. The experimental uncertainty of the

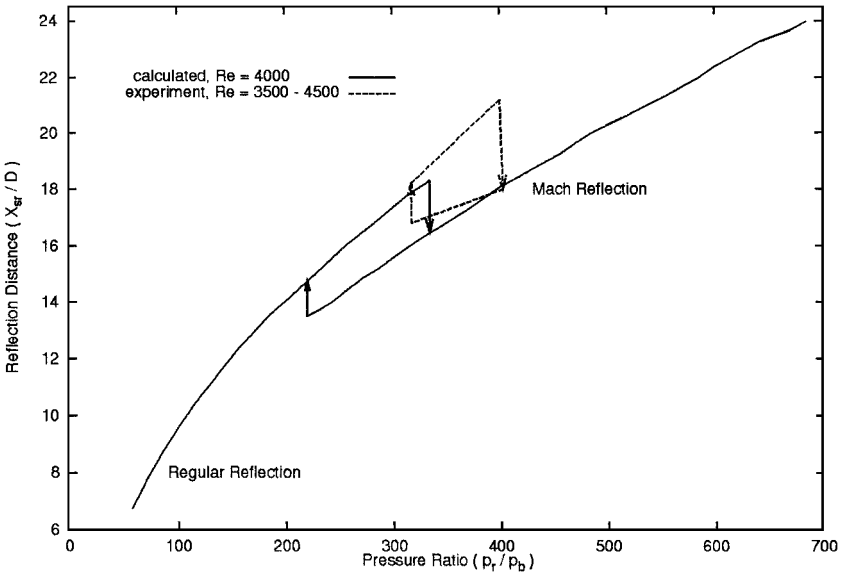

Fig. 4 Reflection distance for range of pressure ratios showing hysteresis loop.

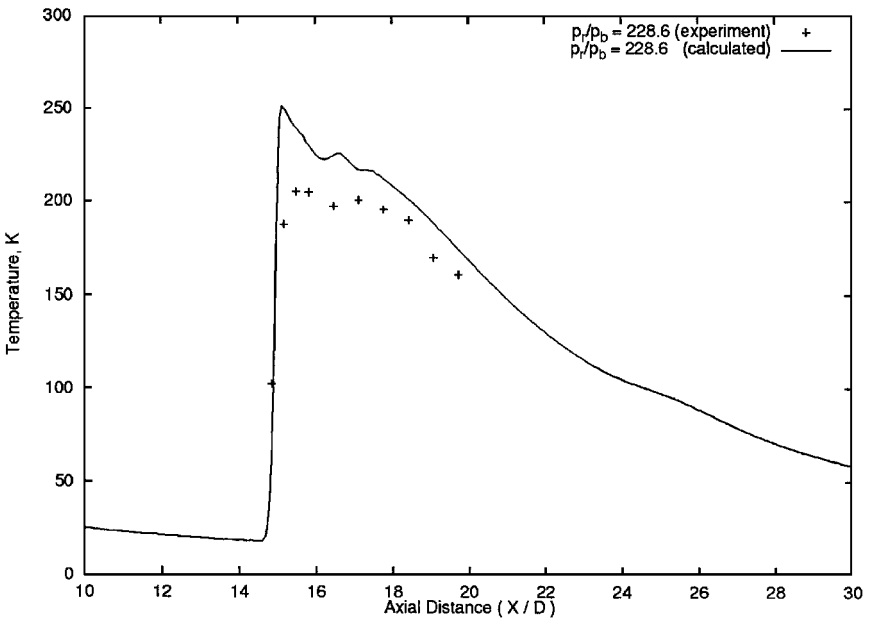

Fig. 5 Centerline temperature: regular reflection.

shock-reflection length corresponds to ±0.33 of the nondimensional length units used in the figure. Given the varying Reynolds number used in the experiment, we cannot expect very close agreement between the CFD and experimental results, and the agreement shown here is considered reasonable. In the case of two-dimensional shock-reflection hysteresis, the limits of the dual-solution domain can be calculated from knowledge of the Mach number upstream of the reflection and the incident shock angle.[1,20,21] In principle a similar analysis is possible here; the Mach number and local shock angle can be obtained from the CFD results, and the theoretical limits to the dual-solution domain can be calculated and compared with the numerical results. However, this approach was not successful because the shock angles are difficult to measure to the necessary degree of accuracy from the field plots caused by curvature of the shock and shock smearing.

Across most of the pressure ratio range, the predicted reflection type matches the experimentally observed type. Very good agreement between calculated and experimental temperature profiles was achieved in these cases. Figures 5–8 show typical comparisons. Note that absolute temperatures are shown here, the ambient temperature being 288 K. The experimental data[7] were obtained using a nonintrusive measurement technique, with an expected accuracy of ±5%. Figures 5 and 6 compare temperature results on the plume centerline and across a radial section, respectively, for a regular reflection at $p_r / p_b = 228.6$. Figure 5 shows a good prediction of the regular reflection location, indicated by the sharp rise in temperature, and downstream of the reflection agreement is also good although temperature is slightly overpredicted. Figure 6 shows good agreement in the temperature profiles at an axial position immediately downstream of the first regular reflection. At the centerline the temperature is high because the gas has been compressed by the incident and reflected shock and has yet to reexpand. Moving across the plume, there is a sharp decrease in temperature as the reflected shock is traversed. The fast moving gas in the shock layer behind the incident shock, which has yet to be processed by the reflected shock, is shown by the temperature trough. The temperature recovers through the shear layer to the ambient value. Figures 7 and 8 compare temperature results on the plume centerline and across a radial section respectively for a Mach reflection at $p_r / p_b = 328.6$. Good agreement is also demonstrated here. Note that in Fig. 7 the

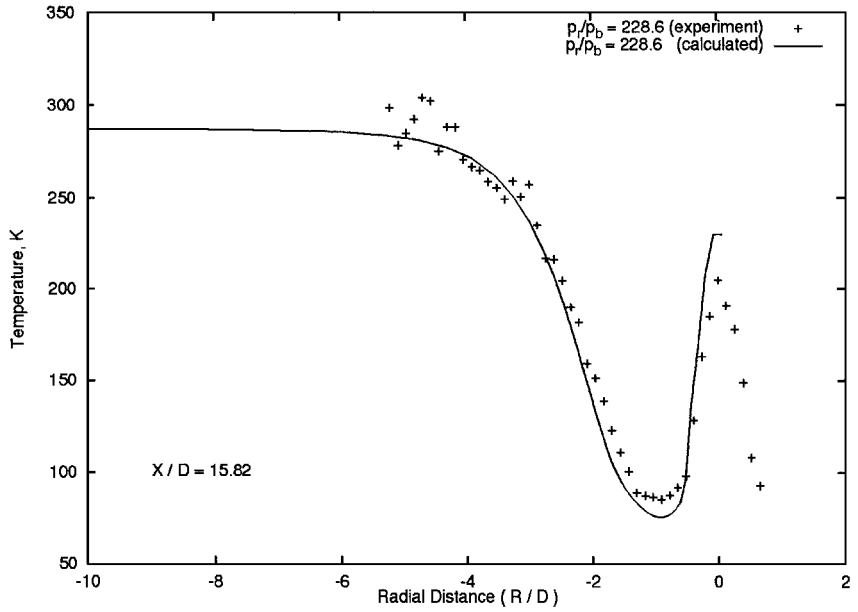

Fig. 6 Temperature profile at X/D = 15.82: regular reflection.

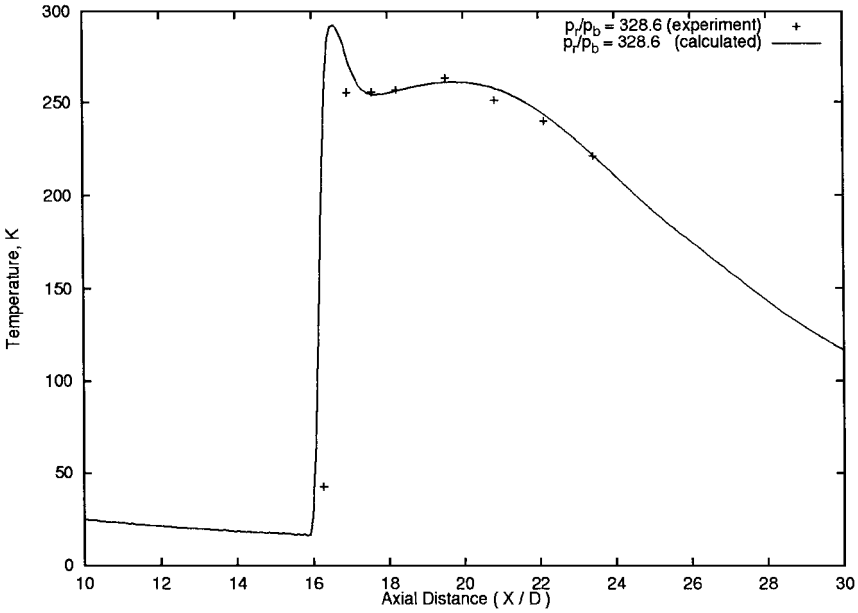

Fig. 7 Centerline temperature: Mach reflection.

calculated temperature reaches the stagnation value of 288 K immediately after the Mach disk, implying that the flow has stagnated. This will be discussed in Sec. IV.B.

Figures 9 and 10 show calculated density contours for both RR and MR for the same pressure ratio ($p_r/p_b = 285.7$), a condition which lies in the dual-solution domain. Upstream of the first shock reflection no difference in the flow behavior can be detected, in accordance with experimental observations. The calculated centerline distributions of all flow variables are identical upstream of the first shock reflection. These figures clearly show that the MR occurs slightly upstream of the corresponding RR, allowing a greater initial expansion in the RR case. The field plots of the calculated results, more of which are presented next, are in very good agreement with the flow visualization photographs from the original experiments.[7]

The grid-convergence study and good agreement obtained, for both shock-reflection distance and temperature values, over a range of pressure ratios and at several different axial stations gives confidence in the accuracy of the calculations. The detail obtained from the CFD study will now be used to examine a number of flow features.

IV. Plume Structure

A. Regular Reflection

Figure 11 shows calculated pressure contours for the pressure ratio $p_r/p_b = 185.7$, which lies in the RR range. The section of the plume shown is centered on the second shock cell and includes the incident shock from the first cell and reflected shock at the beginning of the third. The figure clearly shows the repeated shock cell pattern typical of this regime. From these field plots the important elements of the plume structure can be visualized. On exiting from the nozzle, the air is at a higher pressure than the ambient air and expands sharply, increasing the cross-sectional area of the plume. Expansion waves reflect from the freejet boundary as compression waves, and in so doing turn the jet boundary toward the axis. The curved nature of the jet boundary causes the compression waves to coalesce and form an oblique shock wave, the incident shock labelled. Air passing through this shock is turned back toward the axis and collects in a shock layer of increasing density, causing the shock itself to turn further toward the axis. This is also encouraged by the increasing Mach number of the air before the shock in the still-expanding core flow, whose pressure now lies below

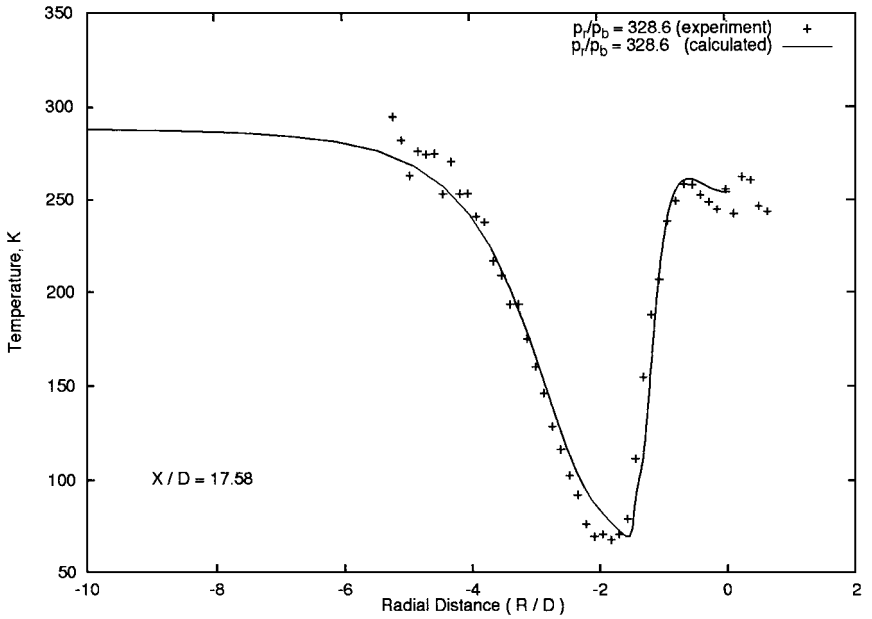

Fig. 8 Temperature profile at $X/D = 17.58$: Mach reflection.

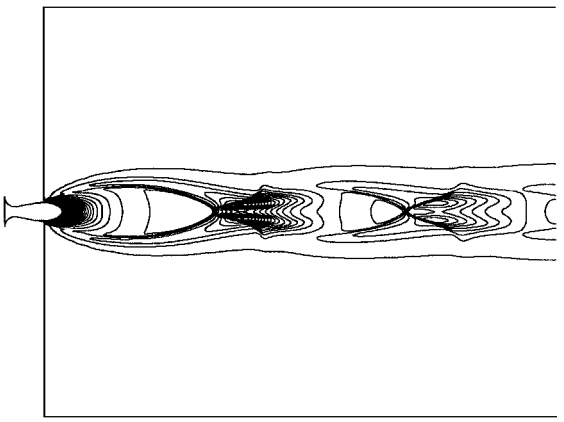

Fig. 9 Density contours showing regular reflection: $p_r/p_b = 285.7$.

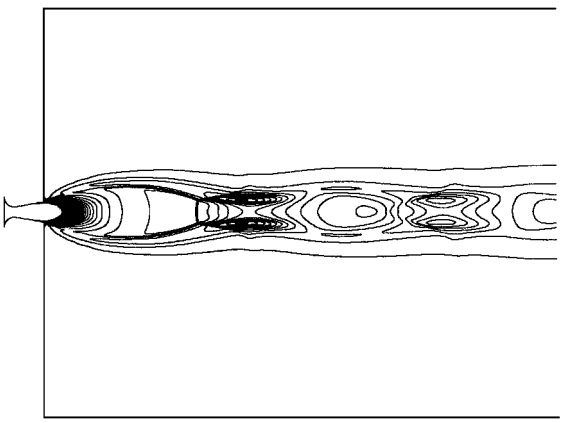

Fig. 10 Density contours showing Mach reflection: $p_r/p_b = 285.7$.

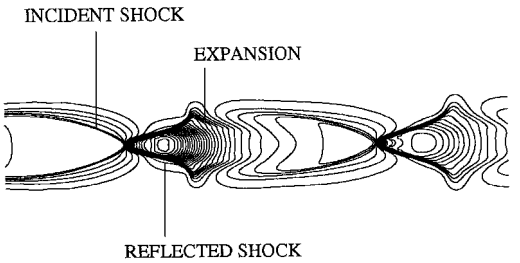

Fig. 11 Pressure contours showing regular reflection: $p_r/p_b = 185.7$.

the background pressure. The axisymmetric shock intersects the axis and is reflected as another oblique shock. The shock reflection is the mechanism through which the condition of axial flow on the centerline is achieved; after the incident shock the flow is converging on the axis and is then turned away by the reflected shock. Immediately downstream of the reflection point the air being processed by the reflected shock is of increasing density because of the accumulated shock layer, turning the shock toward the axis. This tendency is quickly overtaken by the rapidly reexpanding core flow, which causes the shock to turn outward again toward the jet boundary. The change in curvature of the reflected shock is clearly seen in Fig. 11. The shock is reflected as expansion waves by the freejet boundary, which is turned back away from the axis. This expansion reinforces the expansion of the underexpanded core flow and initiates another shock cell when the expansion waves again reflect from the jet boundary. The pattern is repeated, its strength gradually lessening, until the structure is destroyed by diminishing pressure ratio and mixing.

Figures 12 and 13 show calculated centerline distributions of pressure and Mach number. Regular reflections arising for three pressure ratios are shown: $p_r/p_b = 334.3$ is the highest pressure ratio for which regular reflection occurs (a limit of the hysteresis loop), $p_r/p_b = 57.1$ was the lowest pressure ratio considered, and $p_r/p_b = 185.7$ was selected as an intermediate point. The ragged peaks to the pressure curves for the lower pressure ratio cases are possibly explained by the interaction of the shock layer behind the incident shock with the reflected shock. Upstream of the interactions all of the curves are coincident. Despite the fact that the cross-sectional area of the plume increases with pressure ratio, the core expansion along the axis appears to be independent of pressure ratio until the reflection occurs. Before the first shock reflection the gas has become significantly overexpanded, is recompressed by means of the shock waves, then becomes overexpanded again (although less so), and the pattern is repeated. From Fig. 13 one can see that the flow behind the first regular shock reflection may become subsonic. From the present calculations the lowest pressure ratio at which this occurs is $p_r/p_b = 171.4$, and as the pressure ratio increases in the RR range the subsonic region becomes larger and the minimum Mach number smaller. At the upper limit of the RR range ($p_r/p_b = 334.3$), the subsonic region is 2.65 throat diameters in length with a minimum Mach number of 0.26. More will be said about the region of subsonic flow in Sec. IV.C.

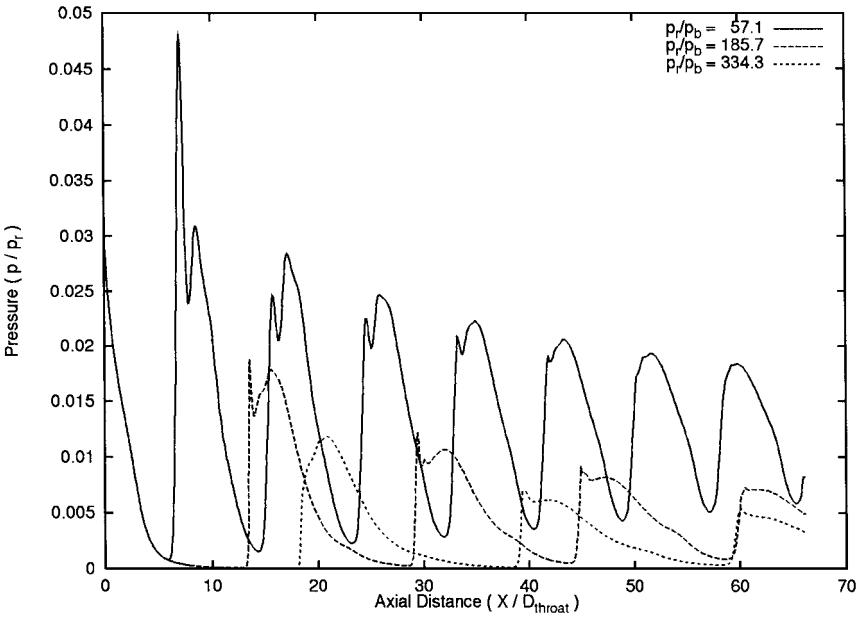

Fig. 12 Centerline pressure: regular reflection.

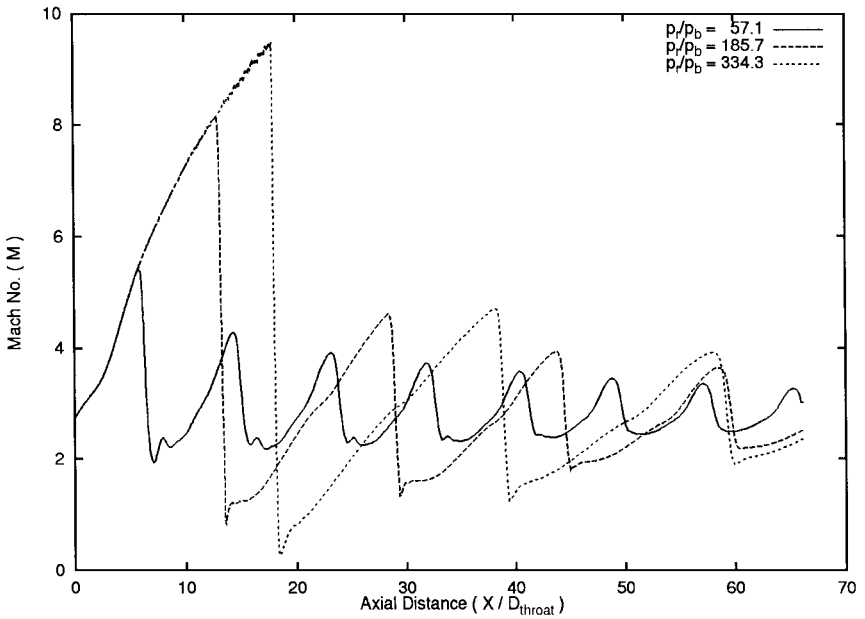

Fig. 13 Centerline Mach number: regular reflection.

B. Mach Reflection

As the ratio of nozzle exit to background pressure increases, the amount of expansion at the nozzle exit increases, and the shock cell grows in size. As the pressure ratio increases, the angle at which the incident shock intersects the axis increases. The increasing angle has the result that the flow behind the incident shock is deflected more toward the centerline. The stronger incident shock also results in a greater decrease in Mach number across the shock, an effect that is countered by a greater Mach number in the core flow upstream of the incident shock. The shock deflection angle necessary for a reflected shock to realign the flow is thus increasing, and at the same time the Mach number between shocks may be decreasing. A point is reached where an oblique shock solution for the required deflection to realign the flow is not possible. The realignment is in this case achieved via a Mach reflection, which consists of a normal shock called a Mach disk and a curved oblique shock (see Figs. 10 and 14). The flow is subsonic behind the Mach disk but is supersonic behind the oblique shock. These areas are separated by a slip line, which emanates from the triple point where all three shocks meet. Downstream of the Mach disk, the flow reexpands to become supersonic and initiates a second shock cell in a similar fashion to the case of regular reflection. As the pressure ratio is increased further, the shock cell grows in size, and the incident shock angle upstream of the triple point continues to steepen.

A recirculation zone was predicted behind the Mach disk (see Fig. 15). This surprising feature has been previously noted in an as yet unpublished CFD study.[22] The recirculation is predicted in the present results for all of the pressure ratios examined in the MR range. At the lower limit of the hysteresis loop ($p_r / p_b = 217.1$), the subsonic region is 5.58 throat diameters in length. At the highest pressure ratio considered ($p_r / p_b = 685.7$) the subsonic region is 8.82 throat diameters in length. As can be seen from Figs. 14 and 16, immediately downstream of the Mach disk the pressure is still increasing; this pressure gradient appears to be driving the recirculation. The initial compression caused by the Mach disk brings the overexpanded gas up to ambient pressure. An explanation for the continuing increase in pressure is that immediately downstream of the Mach disk the gas being processed by the reflected oblique

shock is of relatively high density because of the accumulation in the incident shock layer.

The calculated Mach disk is curved, convex if viewed from upstream, for each of the pressure ratio values examined. The amount of curvature increases slowly with pressure ratio. The curvature is apparent in Figs. 10 and 14. This curvature implies that the flow is being turned away from the axis at the triple point. This corresponds to an inverted Mach reflection, following Hornung's classification.[20] However, because of the curvature of all three shocks and their apparent thickness in the present results, it is difficult to identify precisely the location of the triple point and verify the MR type. The flow direction changes significantly in the locality of the triple point (Fig. 15).

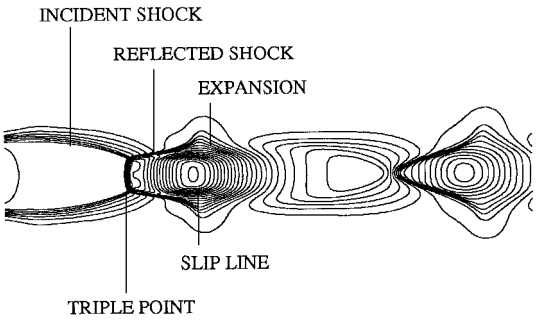

Fig. 14 Pressure contours showing Mach reflection: $p_r/p_b = 342.9$.

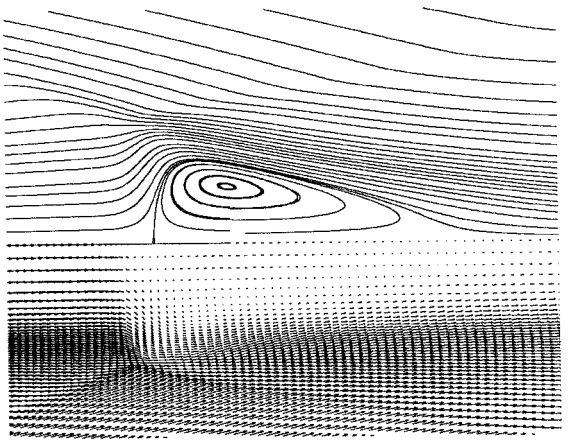

Fig. 15 Velocity vectors and streamlines showing Mach reflection: $p_r/p_b = 342.9$.

Figure 16 shows the calculated centerline pressure distribution. MR results for three pressure ratios are shown: $p_r/p_b = 217.1$ was the lowest pressure ratio for which MR occurs (the lower limit of the hysteresis loop), $p_r/p_b = 685.7$ was the highest pressure ratio considered, and $p_r/p_b = 342.9$ was selected as an intermediate point. As also shown in the RR results, upstream of the interactions all of the curves are coincident.

The shock-reflection type in the subsequent shock cells downstream of the first was calculated to be regular in all cases. However, this study has concentrated on the first shock cell, and no grid-independence study was carried out for the other cells.

C. Pseudo-Mach Reflection

There is some evidence to suggest that the regular reflections discussed in Sec. IV.A are in fact Mach reflections with a Mach disk of small diameter. In Fig. 9 there appears to be a slip line behind the RR; compare with the slip line behind the Mach reflection in Fig. 10. As already noted in Sec. IV.A, there is a significant subsonic region behind the RR at the higher pressure ratios. On close examination of the pressure contours in the region around the reflection (see Fig. 11), there is an apparent Mach disk of approximately three grid cells in radius. Refinement of the grid in this area by a factor of 10 had no impact on this feature. Two different levels of MR are occurring. The incident shock waves to the reflection are curved, and conditions upstream of the shock are varying along the shock; a conventional pressure-deflection diagram approach borrowed from two-dimensional shock reflection analysis indicates the possibility of multiple MR solutions.[1] In addition, there is experimental and numerical evidence to suggest that a true axisymmetric RR cannot exist, and what has previously been accepted as a RR is in fact a very-small-diameter MR.[22,23] This very-small-diameter MR has been termed an apparent RR.

V. Conclusion

A CFD method has been successfully applied to shock-reflection hysteresis in an underexpanded jet. The hysteresis of the shock-reflection type reported in experiment has been predicted. The calculated hysteresis loop agrees well with experimental results. The plume structure has been examined in detail using the results of the CFD analysis for both apparent RR and MR. Good agreement between experimental and CFD results has been demonstrated. The value of a CFD analysis has been demonstrated by the detail that has been obtained from the results, enabling the examination of flow features not initially recognized from the experiments. A recirculation

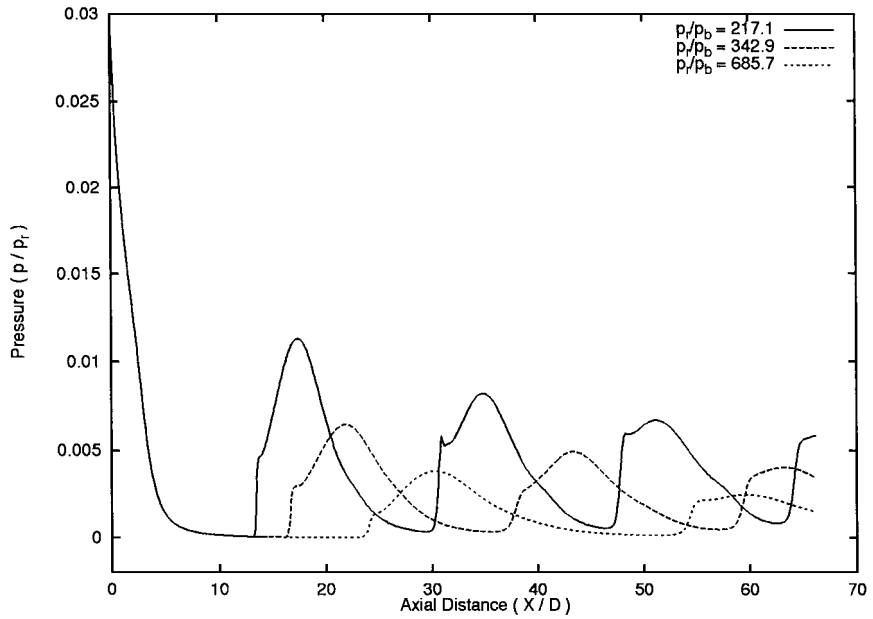

Fig. 16 Centerline pressure: Mach reflection.

zone behind the Mach disk has been predicted, which appears to be driven by a pressure gradient caused by the relatively high-density incident shock layer interacting with the reflected oblique shock. The Mach disk is curved, convex when viewed from upstream. The apparent RR is shown to have the characteristics of a MR with a small-diameter Mach disk.

Acknowledgments

This work is supported by a University of Glasgow scholarship and sponsorship from DERA Bedford. Many thanks to Paul Welsh, Terry Cain, and Martin Gilmore from Aerophysics, DERA Farnborough, for introducing this problem, fruitful discussions during the course of the study, and providing the experimental data. Thanks also to the other members of the CFD group within the Aerospace Engineering Department for their contributions.

References

[1]Gribben, B. J., Badcock, K. J., and Richards, B. E., "Shock Reflection Hysteresis in an Underexpanded Jet: a CFD Study," Univ. of Glasgow, Aerospace Engineering Rept. 9808, Glasgow, Scotland, U.K., April 1998.

[2]Crist, C., Sherman, P. M., and Glass, D. R., "Study of the Highly Underexpanded Sonic Jet," *AIAA Journal*, Vol. 4, No. 1, 1966, pp. 68–71.

[3]Abbett, M., "Mach Disk in Underexpanded Exhaust Plumes," *AIAA Journal*, Vol. 9, No. 3, 1971, pp. 512–514.

[4]Fox, J. H., "On the Structure of Jet Plumes," *AIAA Journal*, Vol. 12, No. 1, 1974, pp. 105–107.

[5]Chang, I. S., and Chow, W. L., "Mach Disk from Underexpanded Axisymmetric Nozzle Flow," *AIAA Journal*, Vol. 12, No. 8, 1974, pp. 1079–1082.

[6]Eastman, D. W., and Radtke, L. P., "Location of the Normal Shock Wave on the Exhaust Plume of a Jet," *AIAA Journal*, Vol. 1, No. 4, 1963, pp. 918, 919.

[7]Welsh, F. P., "Shock Reflection Hysteresis in Low Density Under-Expanded Jets," Defense Evaluation and Research Agency Farnborough, DRA TR DRA/DWS/WX9/CR97361, Farnborough, England, U.K., March 1997.

[8]Ben-Dor, G., "Reconsideration of the-State-of-the-Art of Shock-Wave-Reflection-Phenomenon in Steady Flows," *Japan Society of Mechanical Engineers International Journal Series B*, Vol. 38, No. 3, 1995, pp. 325–334.

[9]Chpoun, A., Passarel, D., Li, H., and Ben-Dor, G., "Reconsideration of Oblique Shock Wave Reflection in Steady Flows Part I: Experimental Investigation," *Journal of Fluid Mechanics*, Vol. 301, Pt. 1, 1995, pp. 19–35.

[10]Vuillon, J., Zeitoun, D., and Ben-Dor, G., "Reconsideration of Oblique Shock Wave Reflection in Steady Flows Part II: Numerical Investigation," *Journal of Fluid Mechanics*, Vol. 301, Pt. 1, 1995, pp. 37–50.

[11]Prudhomme, S. M., and Haj-Hariri, H., "Investigation of Supersonic Underexpanded Jets Using Adaptive Unstructured Finite Elements," *Finite Elements in Analysis and Design*, Vol. 17, Jan. 1994, pp. 21–40.

[12]Cumber, P. S., Fairweather, M., Falle, S. A. E. G., and Giddings, J. R., "Predictions of the Structure of Turbulent, Highly Underexpanded Jets," *Journal of Fluids Engineering*, Vol. 117, Dec. 1995, pp. 599–604.

[13]Hsu, A. T., and Liou, M. S., "Computational Analysis of Underexpanded Jets in the Hypersonic Regime," *Journal of Propulsion and Power*, Vol. 7, No. 2, 1991, pp. 297–299.

[14]Birkby, P., Dent, J. C., and Page, G. J., "CFD Prediction of Turbulent Sonic Underexpanded Jets," *Proceedings of the 1996 ASME Fluids Engineering Summer Meeting*, Pt. 2, American Society of Mechanical Engineers, 1996, pp. 465–470.

[15]Vuillon, J., Zeitoun, D., and Ben-Dor, G., "Reconsideration of Oblique Shock Wave Reflection in Steady Flows. Part II: Numerical Investigation," *Journal of Fluid Mechanics*, Vol. 301, Pt. 1, 1995, pp. 37–50.

[16]Ivanov, M. S., Gimelshein, S. F., and Beylich, A. E., "Hysteresis Effect in Stationary Reflection of Shock Waves," *Physics of Fluids*, Vol. 7, No. 4, 1995, pp. 685–687.

[17]Badcock, K. J., McMillan, W., Woodgate, M. A., Gribben, B. J., Porter, S., and Richards, B. E., "Integration of an Implicit Multiblock Code Into a Workstation Cluster Environment," *Parallel Computational Fluid Dynamics: Algorithms and Results Using Advanced Computers*, edited by P. Schiano, A. Ecer, J. Periaux, and N. Satofuka, Elsevier, Amsterdam, 1996, pp. 408–415.

[18]Dubuc, L., Cantariti, F., Woodgate, M., Gribben, B., Badcock, K. J., and Richards, B. E., "Solution of the Unsteady Euler Equations Using an Implicit Dual-Time Method," *AIAA Journal*, Vol. 36, No. 8, 1998, pp. 1417–1424.

[19]Gribben, B. J., Badcock, K. J., and Richards, B. E., "Application of PMB2D to Axisymmetric Flows," Univ. of Glasgow, Aerospace Engineering Rept. 9812, Glasgow, Scotland, U.K., April 1998.

[20]Hornung, H. G., "Regular and Mach Reflection of Shock Waves," *Annual Review of Fluid Mechanics*, Vol. 18, 1986, pp. 33–58.

[21]Ben-Dor, G., *Shock-Wave Reflection Phenomena*, Springer–Verlag, New York, 1991.

[22]Welsh, F. P., "Dual Solution Shock Reflection and Shock Layer Instability in Under-Expanded Jets," Defense Evaluation and Research Agency Farnborough, TR DERA/WSS/WX9/CR980114/1.1, Farnborough, England, U.K., Jan. 1998.

[23]Molder, S., Gulamhussein, A., Timofeev, E. V., and Voinovich, P. A., "Focusing of Conical Shocks at the Centre-Line of Symmetry," *21st International Symposium on Shock Waves*, Univ. of Queensland, Queensland, Australia, 1997, Paper 5601, URL: http://aerodec.anu.edu.au/~frank/issw21cd.pdf [cited July 1997].

M. Sichel
Associate Editor